

Article

Open Access



A cigarette filter-derived nitrogen-doped carbon nanoparticle coating layer for stable Zn-ion battery anodes

Yi Guo^{1,2}, Cheng Liu³, Lei Xu², Kaixin Huang², Hao Wu¹, Wenlong Cai^{1*}, Yun Zhang¹

¹Department of Advanced Energy Materials, College of Materials Science and Engineering, Sichuan University, Chengdu 610064, Sichuan, China.

²College of Materials Science and Engineering, Sichuan University of Science & Engineering, Zigong 643000, Sichuan, China.

³Institut de Ciència de Materials de Barcelona (ICMAB), CSIC, Campus UAB, Bellaterra 08193, Spain.

*Correspondence to: Dr. Wenlong Cai, Department of Advanced Energy Materials, College of Materials Science and Engineering, Sichuan University, Chengdu 610064, Sichuan, China. E-mail: caiwl@scu.edu.cn

How to cite this article: Guo Y, Liu C, Xu L, Huang K, Wu H, Cai W, Zhang Y. A cigarette filter-derived nitrogen-doped carbon nanoparticle coating layer for stable Zn-ion battery anodes. *Energy Mater* 2022;2:200032. <https://dx.doi.org/10.20517/energymater.2022.45>

Received: 1 Aug 2022 **First Decision:** 9 Aug 2022 **Revised:** 21 Aug 2022 **Accepted:** 22 Aug 2022 **Published:** 2 Sep 2022

Academic Editors: Yuping Wu, Hao Liu **Copy Editor:** Tiantian Shi **Production Editor:** Tiantian Shi

Abstract

Despite the low cost, safety and high theoretical capacity of metallic zinc, zinc anodes face chronic problems, including zinc dendrites, corrosion and side reactions in aqueous zinc-ion batteries (ZIBs). Herein, a nitrogen-doped carbon nanoparticle coating layer derived from discarded cigarette filters is constructed to suppress parasitic side reactions and zinc dendrite growth. The dense coating layer isolates water from the zinc anode, effectively inhibiting side reactions. Furthermore, the special micro-mesoporous structure and sufficient zincophilic groups guarantee uniform Zn stripping/plating. Consequently, durable cycle stability (2400 cycles at a current density of 1 mA cm⁻²) with a stable polarization potential is achieved for symmetrical cells. The coating layer derived in this study therefore has the potential to improve the electrochemical performance of ZIBs.

Keywords: Zinc dendrites, nitrogen-doped carbon nanoparticle coating layer, micro-mesoporous structure, zinc affinity

INTRODUCTION

Due to their intrinsic safety and low cost, aqueous rechargeable batteries have attracted significant research



© The Author(s) 2022. **Open Access** This article is licensed under a Creative Commons Attribution 4.0 International License (<https://creativecommons.org/licenses/by/4.0/>), which permits unrestricted use, sharing, adaptation, distribution and reproduction in any medium or format, for any purpose, even commercially, as long as you give appropriate credit to the original author(s) and the source, provide a link to the Creative Commons license, and indicate if changes were made.



interest in recent years^[1,2]. Due to the natural abundance, two-electron carrier potential, high theoretical capacity (820 mAh g⁻¹ and 5855 mAh cm⁻³), nontoxicity and chemical stability of metallic Zn, aqueous zinc ion batteries (AZIBs) are experiencing vigorous development^[3-5]. However, there are still many obstacles to the practical application of metallic zinc electrodes, including zinc dendrites, side reactions and the sluggish transport of Zn²⁺. To inhibit Zn dendrites and side reactions, successful approaches, such as electrolyte optimization^[6,7], separator modification^[8,9] and the construction of three-dimensional (3D) hosts^[10,11], have been proposed. In particular, building functional protection layers on the surface of a zinc anode by coating or *in situ* deposition can provide uniform carrier or interfacial flux for dense Zn deposition and also isolate the anode from the bulk electrolyte to suppress side reactions^[12,13]. Direct self-assembled MXenes^[14], highly viscoelastic polyvinyl butyral coating films^[15] and *in situ* organic-inorganic hybrid solid electrolyte interphase (SEI)^[16] have been designed to suppress zinc dendrites by regulating the Zn-ion distribution and Zn nucleation. Furthermore, according to recent studies, zincophilic groups involving oxygen^[17], nitrogen^[18] and sulfur-containing groups^[19] can attract Zn²⁺ in the electrolyte and facilitate their uniform transport and deposition. Without deviating from the intrinsic merits of low cost and easy assembly for AZIBs, cost-effective raw materials and uncomplicated manufacturing routes are urgently needed.

Carbon nanomaterials possess the advantages of low toxicity and adjustable structures, including carbon nanotubes and nanofibers, graphene and carbon quantum dots, and are widely used in energy storage technologies, including Li-, K- and Na-ion batteries^[20,21]. Liang *et al.* used N and O co-doped carbon nanofibers as an interlayer for AZIBs to capture Zn ions and promote regular Zn electrodeposition^[22]. Wei and co-workers coated reduced graphene oxide on a Zn anode to boost its cycle stability^[23]. In particular, carbon nanoparticles possess abundant surface functional groups and can be easily modified by heteroatom and surface optimization, suggesting their potential as alternative options for protective materials for Zn anodes. The preparation methods of carbon nanoparticles are diverse; in particular, using biomass materials as the carbon source to prepare carbon nanoparticles is an economical and effective strategy. In this contribution, we prepare carbon nanoparticles (CNPs) and nitrogen-doped carbon nanoparticles (N-CNPs) using discarded cigarette filters (cellulose acetate fiber) as raw materials. The as-obtained N-CNPs with sufficient zincophilic groups and suitable pore sizes are coated on a Zn anode to stabilize its surface. Consequently, we design an N-CNP-modified symmetric cell that exhibits long cycling life (> 1200 h) and a high Coulombic efficiency (CE) of 98%.

EXPERIMENTAL

Chemicals: The 3 M Zn(CF₃SO₃)₂ electrolyte was purchased from Suzhou Duoduo Chemical Technology Co., Ltd. V₂O₅ was purchased from Aladdin. Zn foils (0.1 mm in thickness) and Cu foils (0.02 mm in thickness) were purchased from Alfa Aesar (Wuxi) Biochemical Technology Co., Ltd. The Zn and Cu foils were not physically or chemically treated before use. Other reagents were of analytical grade without further purification and purchased from Chengdu Kelong Chemical Reagents Corporation.

Synthesis of CNPs and N-CNPs: Discarded cigarette filters were collected and thoroughly cleaned with deionized water and then broken into a powder after drying. This cigarette filter powder (500 mg) was dispersed into 30 mL of deionized water and the dispersion liquid was transferred to a 50 mL Teflon-lined stainless-steel autoclave and heated at 200 °C for 12 h. The brown sediment was then washed and dried to obtain the CNPs. To obtain the N-CNPs, 100 mg of urea were added to the as-mentioned dispersion liquid and treated in the same way as the CNPs.

Preparation of V₂O₅ cathode: 0.117 g of ammonium meta-vanadate were added to 20 mL of glycol and then the mixture was stirred for 8 h before being transferred into a 50 mL Teflon-lined stainless-steel autoclave

and heated at 180 °C for 12 h. Finally, it was heated at 500 °C for 2 h in air to obtain a brown V₂O₅ powder. The V₂O₅ cathode was prepared by coating homogeneous slurries composed of an as-prepared V₂O₅ (70 wt.%) powder, super P (20 wt.%) and a polyvinylidene fluoride binder (10 wt.%) dispersed in N-methyl-2-pyrrolidone onto pure Ti foil.

Preparation of N-CNP-Zn anode: N-CNP-Zn was prepared by mixing polyvinylidene difluoride and CNPs at a weight ratio of 1:9 in an appropriate amount of N-methyl pyrrolidone solvent by grinding. The slurry was cast onto bare Zn by a doctor blading method and dried in a vacuum at 60 °C overnight. The thickness of the N-NCP coating layer was ~9 μm.

Assembly of symmetric and full cells: CR2016-type Zn//Zn symmetric coin cells, Zn//Cu half cells and Zn//V₂O₅ full cells were assembled with identical Zn, Cu and V₂O₅ electrodes, a 3 M Zn(CF₃SO₃)₂ electrolyte (50 μL) and glass fiber separators. All batteries were assembled in open-air conditions.

Characterization: The morphologies of the samples were characterized by SEM (Thermo Scientific Apreo 2C). The surface wettability of the samples was performed using a contact angle (CA) measuring system (POWER EACH, China). The phase and structure of the samples were identified by X-ray diffraction (XRD, Bruker DX-1000) with Cu K α radiation from 10° to 80°. X-ray photoelectron spectroscopy (XPS, ESCALAB Xi+, ThermoFisher) measurements were carried out to identify the chemical element composition and distribution on the surfaces of the materials. Fourier transform infrared (FT-IR) spectroscopy was used to obtain the spectra in the range of 4000-400 cm⁻¹ with an IR tracer-100 (Shimadzu). Raman spectroscopy was performed on a Horiba scientific LabRAM HR evolution spectrometer at 200-2000 cm⁻¹ using a laser at 532 nm.

Electrochemical measurements: The galvanostatic charge/discharge measurements were performed using a battery test system (Neware CT-3008W, China). For the testing of CE, Cu foil and Zn plates served as the working and counter electrodes, respectively, and glass fiber paper worked as the separator. Chronoamperogram measurements were conducted in symmetric cells, in which bare Zn foil was used as the working and counter electrodes. Linear polarization measurements were conducted in a three-electrode configuration, in which bare Zn and N-CNP-Zn foils were used as the working electrode, respectively, a platinum plate was used as the counter electrode and a saturated calomel electrode was used as the reference electrode. Electrochemical impedance spectra (EIS) were measured in a frequency range from 100 kHz to 10 mHz with an AC voltage amplitude of 5 mV. Ionic conductivities were measured by block cells and calculated according to $\sigma = l/(R \times S)$, where R represents the resistance according to the EIS measurements, l represents the thickness of the membrane and S represents the contact area.

RESULTS AND DISCUSSION

Discarded cigarette filters are ubiquitous solid waste and are usually made of cellulose acetate fibers [Figure 1A and Supplementary Figure 1]. Hence, as designed in an economical and efficient manner, carbon nanoparticles using discarded cigarette filters as a raw material were prepared. As presented in Figure 1B, crushed cigarette filters were dispersed uniformly into deionized water (urea solution) and transferred to a Teflon-lined stainless-steel autoclave and heated at 200 °C for 12 h to obtain CNPs or N-CNPs. According to the XRD analysis results [Figure 1C], the as-prepared CNPs and N-CNPs are mainly amorphous, with the small diffraction peak at ~25° indexed to graphite carbon, suggesting the partial graphitization of the as-prepared materials^[24]. Furthermore, XPS was conducted for both the CNPs and N-CNPs. In comparison to CNPs, the X-ray photoelectron spectrum of the N-CNPs reveal a distinct N 1s peak and the high-resolution N 1s peak can be divided into three sub-peaks, namely, graphited-N (401.5 eV), pyrrolic-N (400.1 eV) and

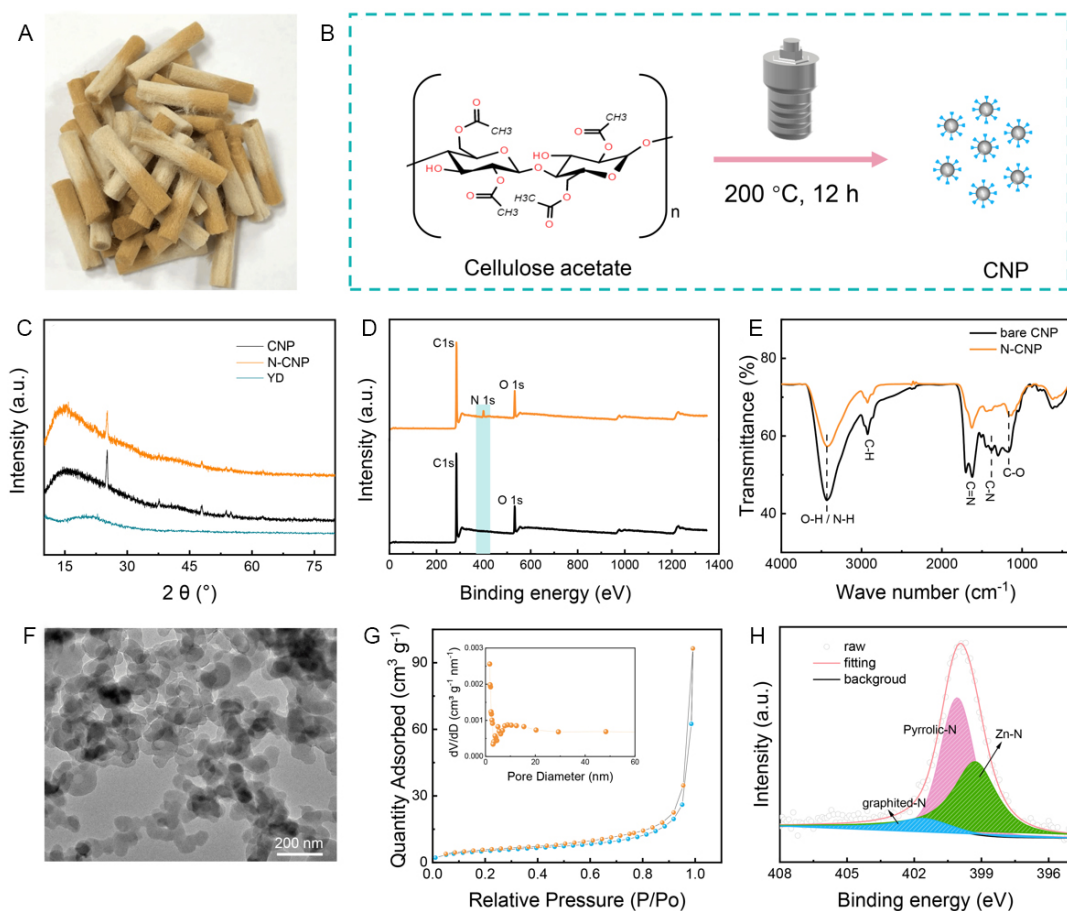


Figure 1. (A) Optical image of discarded cigarette filters. (B) Schematic of preparation process of NCPs/N-NCPs. (C-E) XRD, XPS and FT-IR spectra of CNPs and N-CNPs. (F) TEM image of as-prepared N-CNPs. (G) Nitrogen adsorption/desorption isotherms and pore size distribution (inset) of N-CNPs. (H) X-ray photoelectron spectrum de-convoluted into the N1s of N-CNPs after soaking in the electrolyte.

pyridinic-N (399.8 eV)^[25], as shown in [Figure 1D](#) and [Supplementary Figure 2](#), suggesting that nitrogen was successfully doped into the CNPs. The FT-IR spectrum of the N-CNPs indicates the presence of C-N stretching^[26] at 1386 cm⁻¹ and C=N stretching^[27] at ~1700 cm⁻¹. Moreover, the increased absorption intensity at 3442 cm⁻¹ may be ascribed to the formation of N-H groups, thereby confirming the presence of nitrogen in the N-CNPs [[Figure 1E](#)]. The tiny graphite diffraction peak and abundant oxygen/nitrogen-containing groups indicate the poor conductivity of the N-CNPs, as demonstrated by their Raman spectrum [[Supplementary Figure 3](#)]. Though the peak of the G band is detected at 1580.4 cm⁻¹, the large I_D/I_G ratio suggests a relatively low graphitic order of the N-CNPs^[28].

As examined by transmission electron microscopy (TEM), the as-prepared materials present a nanoparticle morphology with a diameter of ~50 nm [[Figure 1F](#)]. Furthermore, the N₂ adsorption/desorption isotherms and pore size distribution of the N-CNPs are shown in [Figure 1G](#). The isotherm is identified as a type IV hysteresis loop (P/P₀ > 0.6), indicating the presence of a mesoporous structure^[29]. The pore sizes of the N-CNPs are mainly distributed within the range of 1.7 and 11 nm, while the surface area is 19.05 m² g⁻¹, indicating a special microporous-mesoporous structure. Zincophilic groups and special microporous-mesoporous structures are favorable for ion adsorption and shortening the ion transfer paths^[30]. To prove the adsorption of N-CNPs towards Zn²⁺ ions in the electrolyte, a free-standing N-CNP membrane was

soaked into the 3 M $\text{Zn}(\text{CF}_3\text{SO}_3)_2$ electrolyte for a month and examined by XPS after washing. As shown in [Supplementary Figure 4](#), a pair of Zn 2p single peaks at 1045.4 and 1021.68 eV is recorded for the soaked N-CNPs, corresponding to Zn 2p 1/2 and Zn 2p 3/2, respectively. Furthermore, the N 1s spectrum of the N-CNPs illuminates a new peak of 399.2 eV assigned to Zn-N bonds^[31] [[Figure 1H](#)], except for the peaks for graphited-N (401.60 eV) and pyrrolic-N (400.07 eV). This illustrates that the introduction of zincophilic N on the NCPs is conducive to attracting zinc ions.

Based on the properties of N-CNPs and their adsorption ability on zinc ions, an N-CNP artificial interfacial layer is prepared by casting N-CNPs onto a bare Zn anode. As revealed by SEM images [[Figure 2A](#)], the N-CNP-coated Zn exhibits a flat and compact surface with a thickness of $\sim 9 \mu\text{m}$. The CA test results in [Figure 2B](#) show that N-CNP-Zn exhibits a smaller CA of 55° than that of bare Zn (84°) due to the introduction of hydrophilic groups, which is beneficial to the uniform distribution of hydrated zinc ions. However, the improvement in electrolyte affinity does not sacrifice the water resistance of the N-CNP layer. To demonstrate this, bare Zn and N-CNP-Zn-coated Zn foils were immersed into the 3M $\text{Zn}(\text{CF}_3\text{SO}_3)_2$ electrolyte for one week and subsequently investigated by XRD. There are no changes for the N-CNP-protected Zn foil [[Figure 2C](#)], while the bare one after immersion shows obvious side products, including $\text{Zn}(\text{OH})_2 \cdot 0.5\text{H}_2\text{O}$ (JCPDS no. 20-1436) and $\text{Zn}_5(\text{CO}_3)_2(\text{OH})_6$ (JCPDS no. 19-1458)^[32]. In addition, linear polarization experiments are also carried out in a three-electrode system and the results are presented in [Figure 2D](#). The bare Zn shows a corrosion potential of -0.910 V and a corrosion current density of 0.430 mA cm^{-2} , according to the Tafel extrapolation of the polarization curve. In contrast, the N-CNP-Zn manifests a more positive corrosion potential (-0.907 V) and a smaller corrosion current density (0.400 mA cm^{-2}), demonstrating less tendency for corrosion reactions and conforming to the corrosion resistance of the N-CNP coating layer.

Furthermore, the protective layer also assists in regulating ion distribution. According to the ionic conductivity analysis [[Supplementary Figure 5](#)], the layer presents a relatively good ionic conductivity of $\sim 7.1 \times 10^{-5} \text{ S cm}^{-1}$ ^[2]. Moderate ionic conductivity and sufficient zincophilic groups are beneficial to the migration of ions. The Zn^{2+} transference number ($t_{\text{Zn}^{2+}}$) is of importance for electrochemical properties since a high cation transference ability would relieve the concentration gradient at the electrode/electrolyte interface, decrease the anion concentration and inhibit side reactions^[33]. The ($t_{\text{Zn}^{2+}}$) of the N-CNP modified cell is calculated to be 0.85, which is higher than that of bare Zn (0.31), as displayed in [Supplementary Figure 6](#). The large Zn^{2+} transference number can be attributed to the evenly-distributed negative groups and the micro-mesoporous structure of the N-CNP layer, leading to an expressway for cations but a blocked channel for the anions. Before being reduced to Zn, Zn^{2+} needs to overcome an energy barrier, i.e., the nucleation overpotential (NOP). As shown in [Figure 2E](#), the symmetrical cell with an N-CNP layer presents a higher NOP of $\sim 160 \text{ mV}$ compared with the bare one ($\sim 117 \text{ mV}$). A high nucleation overpotential is favorable for the fine-grained Zn deposits^[7], indicating a finer structure of nuclei for the Zn deposition in the N-CNP-Zn electrode system compared to that in bare Zn. The deposition action is also influenced by the Zn growth process. During the plating process, the adsorbed Zn^{2+} on the electrolyte/anode interface can be locally reduced to Zn^0 but also diffuse transversely in the initial nucleation stage to minimize the surface energy^[34]; however, the latter pattern will cause uncontrolled nucleation and significant dendrite growth. Chronoamperometry tests are used to examine the influence of the N-CNP coating layer on the Zn growth pattern, as illustrated in [Figure 2F](#). When an overpotential of -200 mV is applied to the symmetric cells, the current density of the cell without the N-CNP coating layer continues to increase significantly, indicating substantial planar diffusion and rough deposition behavior^[35]. For the cell with N-CNPs, it maintains a dramatically low current, which means that the N-CNP coating layer can induce uniform Zn^{2+} distribution and minimal two-dimensional diffusion by the uniformly distributed zincophilic sites.

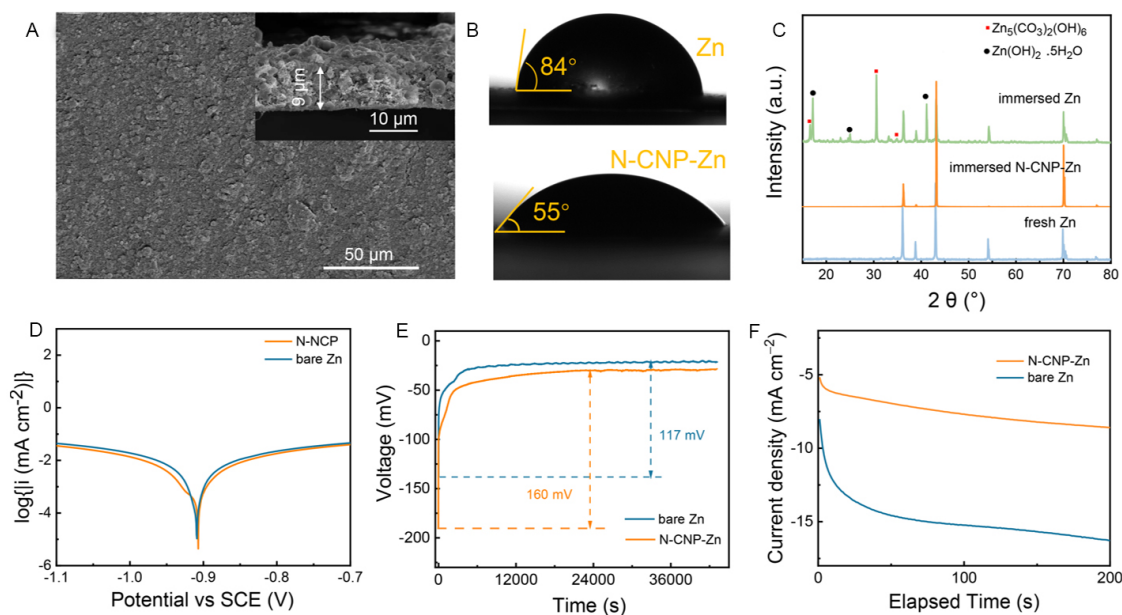


Figure 2. (A) Plane and cross-section (inset) SEM images of N-CNP coating layer. (B) CA test for bare Zn and N-CNP-coated Zn foil. (C) XRD patterns of Zn foil and N-CNP-coated Zn foil after soaking in electrolyte for one week. (D) Linear polarization curves showing the corrosion on bare Zn and N-CNP-coated Zn foil. (E) V-t curves during Zn nucleation and deposition of Zn//Zn symmetric battery with/without N-CNP coating layer. (F) Time-current curves of Zn nucleation and deposition at an overpotential of -200 mV of the symmetric cells with N-CNP-Zn and bare Zn anodes.

The deposition behavior of the bare Zn and N-CNP-coated Zn electrodes is further investigated by inspecting their morphology after deposition for 10, 30 and 60 min at a current density of 2 mA cm⁻². As illustrated in Figure 3A-D, zinc preferentially forms nuclei at thermodynamical sites and gradually develops into zinc dendrites on the bare Zn electrode, which leads to an uncompacted and uneven surface during the whole deposition process, in agreement with the significantly augmented current in the CA tests. Under the protection of the N-CNP coating layer, the electrode presents a compact, uniform and dendrite-free morphology [Figures 3E-G]. At the initial plating stage, the coating layer maintains a similar morphology and thickness as the bare N-CNP layer [Supplementary Figure 7A and B], implying that zinc deposits and grows on the substrate surface. Due to the sufficient zinc ion source provided by the coating layer, newly deposited Zn grows upward and fills the pores of the N-CNP layer without dendrite observation [Figure 3G]. It is noteworthy that subsequent deposition occurs on the not covered substrate (orange circle in Figure 3F) rather than on the surface of the coating layer due to its poor electronic conductivity, leading to a smooth and dense morphology [Figure 3G and H]. The corresponding deposition morphologies are also in situ monitored using an optical microscope coupled with an electrochemical working station. Unsurprisingly, the N-CNP coating layer presents a smooth surface morphology in the whole plating process and the newly deposited Zn layer is also found under the protective layer [Supplementary Figure 8]. Based on the above discussion, the Zn nucleation and growth process on the bare and N-CNP-coated Zn electrodes can be summarized, as illustrated in Figure 3I. The zinc ion distribution beneath the N-CNP layer is more uniform than that on the bare Zn electrode, due to the good zinc affinity and the micro-mesoporous structure, which induces uniform zinc nucleation and 3D growth. The as-deposited Zn grows upward and fills the coating layer and forms a compact and uniform deposition layer. In contrast, without the protection of the N-CNP coating layer, the planar diffusion of zinc ions and the preferential nucleation at suitable sites can be detected on the bare Zn anode, finally causing the aggregation of by-products and the growth of dendrites.

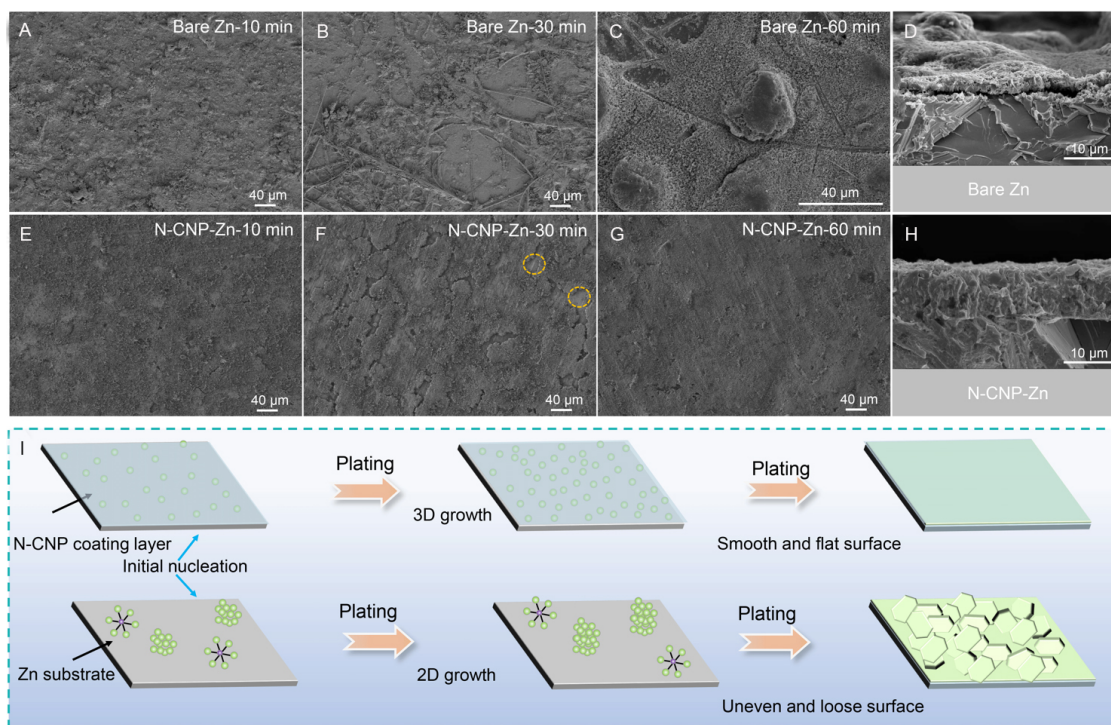


Figure 3. (A-D) Deposition morphology of Zn electrode after depositing for 10, 30 and 60 min and corresponding cross-section morphology. (E-H) Deposition morphology of N-CNP-Zn electrode after depositing for 10, 30, and 60 min and corresponding cross-section morphology. (I) Schematic illustration of Zn nucleation and deposition process for bare Zn and N-CNP-Zn electrodes.

Considering the desirable properties of N-CNP-Zn confirmed above, the long-term galvanostatic cycling of symmetrical Zn cells is carried out to further evaluate its practicability. As depicted in [Figure 4A](#), the symmetrical cell with an N-CNP layer shows a stable cycling life of 1200 h (2400 cycles) at a current density of 1 mA cm^{-2} and an area capacity of 1 mAh cm^{-2} . Moreover, the voltage hysteresis of the N-CNP-Zn electrode increases slowly with increasing cycling (inset of [Figure 4A](#)). In contrast, short-circuit occurs after only 90 h for the bare Zn cells [[Supplementary Figure 9](#)]. The improved cycling stability should be attributed to the enhanced zinc affinity and the shortened ion migration paths. Therefore, the N-CNP-Zn electrode can steadily operate when the current density increases from 0.5 to 5 mA cm^{-2} with a minor increased polarization voltage [[Figure 4B](#)], which largely relies on promoted corrosion resistance and uniform Zn^{2+} diffusion enabled by the N-CNP coating layer. When the current density increases to 3 mA cm^{-2} , the modified cells can still work stably for more than 300 h [[Figure 4C](#)] at an area capacity of 3 mAh cm^{-2} , proving the excellent stability of N-CNP-Zn in stripping/plating.

To investigate the application potential of N-CNP-Zn, Zn//Cu half cells with bare and coated Zn electrodes are assembled and their CE is examined. As presented in [Figure 4D](#), the modified cell exhibits outstanding cycling stability (over 500 h) with an average CE of 98.08% at a current density of 3 mA cm^{-2} , while the bare Zn cells only steadily cycle for 60 h. Additionally, the cell decorated by N-CNP exhibits a low voltage hysteresis of 154 mV during 400 cycles, confirming the suppressed side reactions and controllable zinc ion distribution [[Figure 4E](#)]. The capability of N-CNP-Zn anodes is explored by characterizing the electrochemical performance of Zn// V_2O_5 full batteries. V_2O_5 is a promising cathode material for AZIBs; herein, a kind of V_2O_5 rod is prepared by a simple hydrothermal method and used as the cathode material. Its structure and morphology are detected by XRD and SEM [[Supplementary Figure 10A and B](#)]. As shown, all the diffraction peaks of the as-prepared V_2O_5 are well indexed to V_2O_5 (JCPDS card no. 41-1426),

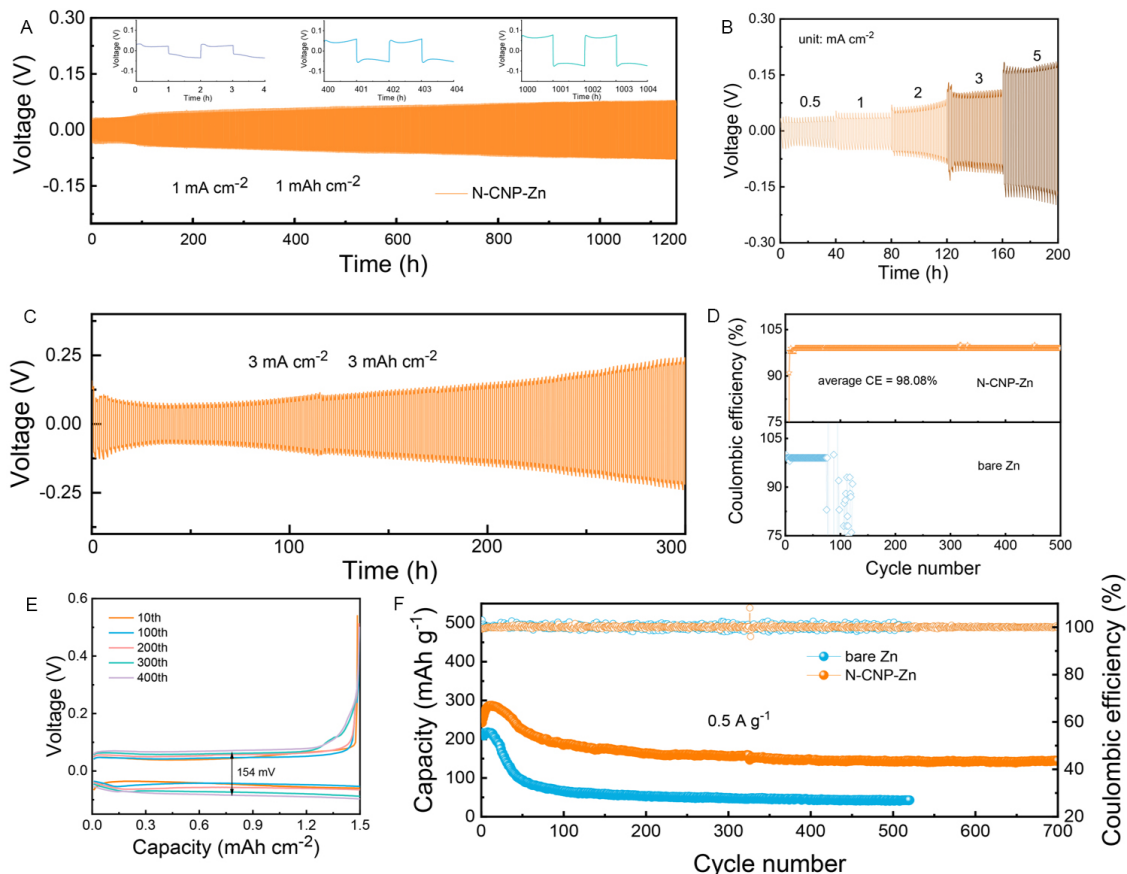


Figure 4. (A) V-t curves of N-CNP-Zn//N-CNP-Zn symmetric cells during plating/stripping process. (B) Rate performance of symmetric cell with N-CNP-Zn electrode. (C) Cycling performance of N-CNP-Zn//N-CNP-Zn symmetric cells at a high area capacity of 3 mAh cm⁻². (D) CE curves of Zn//Cu cells with and without N-CNP coating layer. (E) Charge/discharge curves of N-CNP-Zn//Cu cell at 3 mAh cm⁻². (F) Cycling performance of Zn//V₂O₅ full cells with bare Zn and N-CNP-Zn at a current density of 0.5 A g⁻¹.

showing a high degree of crystallization and the high purity of the samples^[36]. The as-prepared V₂O₅ presents a rod-like structure and gathers into large flakes. **Figure 4F** shows the galvanostatic discharge/charge profiles of two kinds of full cells at a current density of 0.5 A g⁻¹. The full cell with the N-CNP-Zn anode delivers a specific capacity of 144 mAh g⁻¹ after 700 cycles and stable CE, which is much higher than that of the full cell with bare Zn anode. The promotion in electrochemical performance should be assigned to the stable Zn anode and fast ion kinetics enabled by the N-CNP coating layer.

CONCLUSIONS

A zincophilic coating layer with N-CNPs is built on a Zn electrode surface to obtain a remarkably improved durability of rechargeable AZIBs. The N-CNP coating layer serves as an artificial SEI to isolate water in the electrolyte and regulate the Zn²⁺ distribution, leading to no by-products and a dendrite-free plating/stripping action. The coating layer has good hydrophilicity and a large specific surface area derived from the uniformly distributed hydrophilic sites (oxygen/nitrogen-containing groups) and its nanostructure, which ensures the homogeneous distribution of hydrated zinc ions and open pathways for Zn²⁺ migration. As a result, symmetrical cells with the N-CNP-coated Zn electrode offer stable plating/stripping performance with an overpotential (< 200 mV) after a long lifespan of 1200 h at 1 mA cm⁻² (1 mAh cm⁻²). The Zn//V₂O₅ full cell with the N-CNP-coated Zn anode exhibits a higher discharge capacity than a bare full cell at a current density of 0.5 A g⁻¹, due to the stable Zn anode and fast ion transfer kinetics.

DECLARATIONS

Acknowledgments

The authors thank teacher Yingdong Peng for offering waste cigarette filters.

Authors' contributions

Methodology, formal analysis, investigation, writing manuscript: Guo Y, Cai WL

Formal analysis: Liu C, Xu L, Huang KX

Supervision: Wu H, Zhang Y

Availability of data and materials

The data supporting our work can be found in the supplementary information.

Financial support and sponsorship

This work is supported by the Talents Program of Sichuan University of Science & Engineering (2019RC01); the Innovation and Entrepreneurship Training Program for College Students at Sichuan University of Science & Engineering (cx2020004); the National Key Research and Development Program of China (2018YFB0104200).

Conflicts of interest

All authors declared that there are no conflicts of interest.

Ethical approval and consent to participate

Not applicable.

Consent for publication

Not applicable.

Copyright

© The Author(s) 2022.

REFERENCES

1. Xu J, Ji X, Zhang J, et al. Aqueous electrolyte design for super-stable 2.5 V $\text{LiMn}_2\text{O}_4 \parallel \text{Li}_4\text{Ti}_5\text{O}_{12}$ pouch cells. *Nat Energy* 2022;7:186-93. DOI
2. Hao J, Li B, Li X, et al. An in-depth study of Zn metal surface chemistry for advanced aqueous Zn-ion batteries. *Adv Mater* 2020;32:e2003021. DOI PubMed
3. Zhang Y, Bi S, Niu Z, Zhou W, Xie S. Design of Zn anode protection materials for mild aqueous Zn-ion batteries. *Energy Mater* 2022;2:200012. DOI
4. Li Y, Yang W, Han L, et al. Recent progress and perspective of multifunctional integrated zinc-ion supercapacitors. *Energy Mater* 2022;2:200018. DOI
5. Liu Y, Hu J, Lu Q, et al. Highly enhanced reversibility of a Zn anode by in-situ texturing. *Energy Stor Mater* 2022;47:98-104. DOI
6. Cao L, Li D, Deng T, Li Q, Wang C. Hydrophobic organic-electrolyte-protected zinc anodes for aqueous zinc batteries. *Angew Chem Int Ed* 2020;59:19292-6. DOI PubMed
7. Zhang Y, Zhu M, Wu K, et al. An in-depth insight of a highly reversible and dendrite-free Zn metal anode in a hybrid electrolyte. *J Mater Chem A* 2021;9:4253-61. DOI
8. Cao J, Zhang D, Gu C, et al. Modulating Zn deposition via ceramic-cellulose separator with interfacial polarization effect for durable zinc anode. *Nano Energy* 2021;89:106322. DOI
9. Qin Y, Liu P, Zhang Q, et al. Advanced filter membrane separator for aqueous zinc-ion batteries. *Small* 2020;16:e2003106. DOI PubMed
10. Zhang Q, Luan J, Fu L, et al. The three-dimensional dendrite-free zinc anode on a copper mesh with a zinc-oriented polyacrylamide electrolyte additive. *Angew Chem Int Ed* 2019;58:15841-7. DOI PubMed
11. Kang Z, Wu C, Dong L, et al. 3D porous copper skeleton supported zinc anode toward high capacity and long cycle life zinc ion batteries. *ACS Sustainable Chem Eng* 2019;7:3364-71. DOI

12. Liu X, Lu Q, Yang A, Qian Y. High ionic conductive protection layer on Zn metal anode for enhanced aqueous zinc-ion batteries. *Chinese Chem Lett* 2022. DOI
13. Lu Q, Liu C, Du Y, et al. Uniform Zn deposition achieved by Ag coating for improved aqueous zinc-ion batteries. *ACS Appl Mater Interfaces* 2021;13:16869-75. DOI PubMed
14. Zhang N, Huang S, Yuan Z, Zhu J, Zhao Z, Niu Z. Direct self-assembly of MXene on Zn anodes for dendrite-free aqueous zinc-ion batteries. *Angew Chem Int Ed* 2021;60:2861-5. DOI PubMed
15. Hao J, Li X, Zhang S, et al. Designing dendrite-free zinc anodes for advanced aqueous zinc batteries. *Adv Funct Mater* 2020;30:2001263. DOI
16. Di S, Nie X, Ma G, et al. Zinc anode stabilized by an organic-inorganic hybrid solid electrolyte interphase. *Energy Stor Mater* 2021;43:375-82. DOI
17. Cao J, Zhang D, Gu C, et al. Manipulating crystallographic orientation of zinc deposition for dendrite-free zinc ion batteries. *Adv Energy Mater* 2021;11:2101299. DOI
18. Xie F, Li H, Wang X, et al. Mechanism for zincophilic sites on zinc-metal anode hosts in aqueous batteries. *Adv Energy Mater* 2021;11:2003419. DOI
19. An Y, Tian Y, Liu C, Xiong S, Feng J, Qian Y. Rational design of sulfur-doped three-dimensional Tix MXene/ZnS heterostructure as multifunctional protective layer for dendrite-free zinc-ion batteries. *ACS Nano* 2021;15:15259-73. DOI PubMed
20. Guo R, Li L, Wang B, et al. Functionalized carbon dots for advanced batteries. *Energy Stor Mater* 2021;37:8-39. DOI
21. Duan Y, You G, Sun K, et al. Advances in wearable textile-based micro energy storage devices: structuring, application and perspective. *Nanoscale Adv* 2021;3:6271-93. DOI
22. Liang Y, Wang Y, Mi H, et al. Functionalized carbon nanofiber interlayer towards dendrite-free, Zn-ion batteries. *Chem Eng J* 2021;425:131862. DOI
23. Shen C, Li X, Li N, et al. Graphene-boosted, high-performance aqueous zn-ion battery. *ACS Appl Mater Interfaces* 2018;10:25446-53. DOI PubMed
24. Yan Z, Yang Q, Wang Q, Ma J. Nitrogen doped porous carbon as excellent dual anodes for Li- and Na-ion batteries. *Chinese Chem Lett* 2020;31:583-8. DOI
25. Yun S, Kang ES, Choi J. Zn-assisted modification of the chemical structure of N-doped carbon dots and their enhanced quantum yield and photostability. *Nanoscale Adv* 2022;4:2029-35. DOI
26. Thirumal V, Pandurangan A, Jayavel R, Krishnamoorthi S, Ilangovan R. Synthesis of nitrogen doped coiled double walled carbon nanotubes by chemical vapor deposition method for supercapacitor applications. *Curr Appl Phys* 2016;16:816-25. DOI
27. Zhang J, Cai T, Li H, Zhao H. Synthesis g-C₃N₄ of high specific surface area by precursor pretreatment strategy with SBA-15 as a template and their photocatalytic activity toward degradation of rhodamine B. *Phosphorus, Sulfur Silicon Relat Elem* 2019;194:229-35. DOI
28. Pantea D, Darmstadt H, Kaliaguine S, Sümmchen L, Roy C. Electrical conductivity of thermal carbon blacks. *Carbon* 2001;39:1147-58. DOI
29. Chen H, Zhou W, Zhu D, et al. Porous cube-like Mn₃O₄@C as an advanced cathode for low-cost neutral zinc-ion battery. *J Alloys Compd* 2020;813:151812. DOI
30. Zhou X, Cao P, Wei A, et al. Driving the interfacial ion-transfer kinetics by mesoporous TiO₂ spheres for high-performance aqueous Zn-ion batteries. *ACS Appl Mater Interfaces* 2021;13:8181-90. DOI PubMed
31. Jia H, Qiu M, Lan C, et al. Advanced zinc anode with nitrogen-doping interface induced by plasma surface treatment. *Adv Sci* 2022;9:e2103952. DOI PubMed PMC
32. He H, Liu J. Suppressing Zn dendrite growth by molecular layer deposition to enable long-life and deeply rechargeable aqueous Zn anodes. *J Mater Chem A* 2020;8:22100-10. DOI
33. Yan H, Li S, Nan Y, Yang S, Li B. Ultrafast zinc-ion-conductor interface toward high-rate and stable zinc metal batteries. *Adv Energy Mater* 2021;11:2100186. DOI
34. Deng C, Xie X, Han J, et al. A Sieve-functional and uniform-porous kaolin layer toward stable zinc metal anode. *Adv Funct Mater* 2020;30:2000599. DOI
35. Zhao Z, Zhao J, Hu Z, et al. Long-life and deeply rechargeable aqueous Zn anodes enabled by a multifunctional brightener-inspired interphase. *Energy Environ Sci* 2019;12:1938-49. DOI
36. Qi Z, Xiong T, Chen T, et al. Harnessing oxygen vacancy in V₂O₅ as high performing aqueous zinc-ion battery cathode. *J Alloys Compd* 2021;870:159403. DOI